Received: 15 April 2019 | Accepted: 12 December 2019

DOI: 10.1002/jor.24583

Journal of Orthopaedic Research®

RESEARCH ARTICLE

Orbital seeding of mesenchymal stromal cells increases osteogenic differentiation and bone-like tissue formation

Johanna Melke[1,2] | Feihu Zhao[1,2] | Keita Ito[1,2] | Sandra Hofmann[1,2]

[1]Orthopaedic Biomechanics, Department of Biomedical Engineering, Eindhoven University of Technology, Eindhoven, The Netherlands

[2]Institute for Complex Molecular Systems, Eindhoven University of Technology, Eindhoven, The Netherlands

Correspondence
Sandra Hofmann, Eindhoven University of Technology, De Rondom 70, 5612AP Eindhoven, The Netherlands.
Email: s.hofmann@tue.nl

Funding information
FP7 Ideas: European Research Council, Grant/Award Number: 336043

Abstract

In bone tissue engineering (TE), an efficient seeding and homogenous distribution of cells is needed to avoid cell loss and damage as well as to facilitate tissue development. Dynamic seeding methods seem to be superior to the static ones because they tend to result in a more homogeneous cell distribution by using kinetic forces. However, most dynamic seeding techniques are elaborate or require special equipment and its influence on the final bone tissue-engineered construct is not clear. In this study, we applied a simple, dynamic seeding method using an orbital shaker to seed human bone marrow–derived mesenchymal stromal cells (hBMSCs) on silk fibroin scaffolds. Significantly higher cell numbers with a more homogenous cell distribution, increased osteogenic differentiation, and mineral deposition were observed using the dynamic approach both for 4 and 6 hours as compared to the static seeding method. The positive influence of dynamic seeding could be attributed to both cell density and distribution but also nutrient supply during seeding and shear stresses (0.0-3.0 mPa) as determined by computational simulations. The influence of relevant mechanical stimuli during seeding should be investigated in the future, especially regarding the importance of mechanical cues for bone TE applications. Our results highlight the importance of adequate choice of seeding method and its impact on developing tissue-engineered constructs. The application of this simple seeding technique is not only recommended for bone TE but can also be used for seeding similar porous scaffolds with hBMSCs in other TE fields.

KEYWORDS
bone, modeling, osteoblasts, stem cells, tissue engineering

1 | INTRODUCTION

Tissue engineering (TE) is an important discipline in regenerative medicine and uses a synergistic combination of biomaterials, cells, and inductive cues to regenerate damaged or defective tissues and create tissue models to study tissue development and disease.[1–3] Seeding cells onto a 3D scaffold is the first step for engineering a tissue-like structure and will determine how many cells attach to the surface of the scaffold and how they are distributed over the 3D volume. Cell distribution and density throughout the scaffold is critical for tissue development as it has been shown to influence cell proliferation, migration, differentiation, and morphological development.[4–6]

Optimization of the seeding process has been addressed before to allow a maximal use of donor cells, maintain cell viability, and provide spatially uniform distribution of cells in the developing tissue.[7,8] These methods can be simply divided into two approaches: static and dynamic

seeding techniques. The most commonly used and simplest method to seed cells onto 3D scaffolds for TE is static seeding, in which a cell suspension is passively pipetted on top of a scaffold, resulting in an inhomogeneous cell distribution and low seeding numbers.[9,10] In contrast to static seeding, various dynamic seeding methods using kinetic forces have been shown to have the potential to improve both seeding efficiency and uniformity of the cell distribution (Table 1).

Uniformly distributed cells are crucial in TE as an inhomogeneous cell distribution will inevitably lead to varying local cell densities within the scaffold volume.[11,12] An initial homogeneous cell distribution has been shown to establish a template for spatially uniform extracellular matrix (ECM) deposition in subsequent culture.[13]

Most dynamic seeding techniques are elaborate or require special equipment (Table 1). In addition, most of these studies focus on the initial seeding density and/or cell distribution after seeding while neglecting their influence on the final tissue outcome.[14–16] In this study, we applied a dynamic seeding method using an ordinary orbital shaker to seed human bone marrow–derived mesenchymal stromal cells (hBMSCs) on silk fibroin (SF) scaffolds for bone TE applications. We hypothesized that this simple seeding method, providing kinetic forces and access to nutrients, will provide a homogenous initial cell distribution and higher cell density compared to static seeding. A homogenous initial cell distribution and higher cell density was expected to be beneficial for the construct's ability to ultimately differentiate along the osteogenic lineage and form mineralized tissue.

2 | MATERIALS AND METHODS

2.1 | Computational fluid dynamics model

To quantify the shear stresses imparted on cells during dynamic cell seeding, a computational fluid dynamics (CFD) model was developed to simulate the orbital shaking system. This system had an orbital radius (R) of 5.0 mm and speed of 150 rpm. In our cell seeding experiment, 4.0 mL of medium were added to the tube (inner diameter =28 mm, Figure 1), resulting in an initial medium height of 15.7 mm. We modeled a bottom section of the tube (height =25 mm, Figure 1), where the scaffold was placed. The cylindrical SF scaffold used in our study had the same geometric features as described previously (diameter: 5 mm, height: 3 mm, porosity: 90%, average pore diameter: 275 μm).[18] The SF scaffold geometry was highly irregular and complex. To save computational costs, the scaffold was homogenized and modeled as porous media with a permeability of 4.27×10^{-10} m^2, which was derived from our previous study.[19] The flow in the porous media domain follows Darcy's law.[20,21] The medium was modeled as an incompressible Newtonian fluid with a dynamic viscosity (μ) of 1.0 mPa.s as described previously.[22] To determine the flow type (laminar or turbulence), the Reynolds number (Re) was calculated using Equation (1):

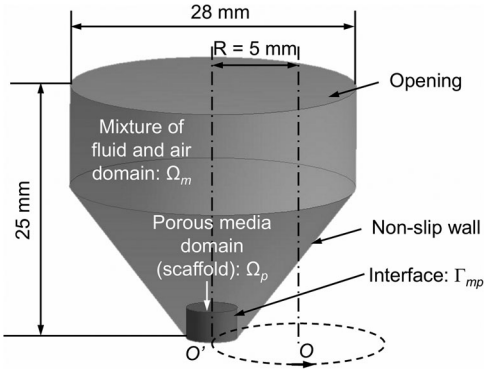

FIGURE 1 Geometry of computational fluid dynamics model for a dynamic seeding system using an orbital shaker

$$Re = \frac{4\rho\omega R^2}{\mu}, \quad (1)$$

where ρ is the medium density ($\rho = 1000$ kg/m^3) and ω is the rotational speed ($\omega = 5\pi$ rad/s).

TABLE 1 Comparison of dynamic seeding techniques

Method	Advantage	Disadvantage	Ref
Filtration/Suction	High seeding efficiency, simple	Homogenous cell distribution not quantified	Li et al[7]
Compress-ion/Suction	Homogenous cell distribution, high cell viability, fast	No comparison to static seeding, elaborate seeding device	Xie et al[14]
Spinner Flask	High seeding efficiency, continuous perfusion of cell suspension	Homogenous cell distribution not quantified	Unsworth et al[15]
Perfusion	Continuous perfusion of cell suspension, homogenous cell distribution, high seeding efficiency	Elaborate seeding device	Wendt et al,[13] Alvarez-Barreto et al[16]
Centrifugation	Homogenous cell distribution	Low cell viability, damages scaffold	Thevenot et al[9]
Orbital shaker	Continuous perfusion of cell suspension, simple, homogenous cell distribution	Requires highly interconnected and open pores structures	Thevenot et al[9]
Magnetic	High seeding efficiency	Elaborate cell labeling, homogenous cell distribution not quantified	Shimizu et al[17]

The *Re* number was approximately 1570, which could result in a turbulent flow.[23] Therefore, according to Cherng et al,[23] a standard κ-epsilon turbulence model was selected and applied to the domain of fluid–air mixture (Ω_m; Figure 1). The pressure drop across the medium-air interface was expressed by the radius and the surface tension using Equation 2:

$$p_M - p_A = \beta\left(\frac{1}{r_M} + \frac{1}{r_A}\right), \tag{2}$$

where, p_M and p_A are the pressures measured by the surface curvature in the normal direction to the interface in liquid (medium) and gas (air) phases, respectively; β is the surface tension of the medium ($\gamma = 0.072$ N/m)[23]; r_M and r_A are the radii measured by the surface curvature in the normal direction to the interface in liquid (medium) and gas (air) phases, respectively.

To track the medium-air interface during shaking, a volume of fluid technique introduced in previous studies[24,25] was used in our CFD model. In each computational finite volume at the interface, the continuity and momentum equations were solved based on the modified definition of the fluid properties (P) in Equation 3[23,24]:

$$\begin{cases} P = \alpha_M \cdot P_M + \alpha_A \cdot P_A \\ \alpha_M + \alpha_A = 1 \end{cases} \tag{3}$$

where P_M and P_A are the properties of medium and air (ie, density and dynamic viscosity) while α_M and α_A are the volume fraction of medium and air, respectively.

In the CFD model, a no-slip boundary condition was assigned to the tube walls, and an opening boundary was defined at the top surface with a relative pressure of 0 Pa (Figure 1). The interface between free fluid and porous media domains followed the condition of continuity of mass flux.[19] The resultant shear stress (τ) in the porous media (homogenized scaffold) domain was calculated by Equation (4):

$$\tau = \mu \cdot \dot{\gamma}|_{\Omega_p}, \tag{4}$$

where $\dot{\gamma}$ is shear rate calculated by finite volume method (FVM) in ANSYS CFX (ANSYS Inc, PA), while Ω_p represents the porous media domain (Figure 1).

Both mixed fluid-air domain and porous media domain were meshed by a tetrahedron method with a patch-conforming algorithm. A total of 1 431 918 elements discretized the whole model geometry. Transient analysis was used in the simulation with a time step of 0.02 seconds for a total time length of 2.8 seconds. Finally, the CFD model was solved by FVM using ANSYS CFX under the convergence criteria of root-mean-square residual of the mass and momentum $<10^{-4}$.

2.2 | Materials

Dulbecco's modified Eagle's medium (DMEM; Cat. No. 41966), antibiotic/antimycotic (Anti-Anti), trypsin-ethylenediaminetetraacetic acid (0.25%) and the Quant-iT PicoGreen dsDNA Assay Kit were from Life Technologies (Bleiswijk, The Netherlands). Methanol (MeOH) was from Merck (Schiphol-Rijk, The Netherlands). Bombyx mori L. silkworm cocoons were purchased from Tajima Shoji Co., Ltd (Yokohama, Japan). All other substances were of analytical or pharmaceutical grade and obtained from Sigma Aldrich (Zwijndrecht, The Netherlands).

2.3 | Scaffold fabrication

SF scaffolds were produced as previously described.[26,27] Briefly, Bombyx mori L. silkworm cocoons were boiled in 0.2M Na_2CO_3 twice for 1 hour. Dried silk was dissolved in 9M LiBr and dialyzed against ultra-pure water (UPW) using SnakeSkin Dialysis Tubing (molecular weight cutoff: 3.5 kDa; Thermo Fisher Scientific, Breda, The Netherlands). Dialyzed silk solution was frozen, lyophilized, and dissolved in 1,1,1,3,3,3-Hexafluoro-2-propanol (HFIP), resulting in a 17% (w/v) solution. One milliliter silk-HFIP solution was added to 2.5 g NaCl with a granule size between 250 and 300 μm in a Teflon container and allowed to air dry. Silk-salt blocks were immersed in 90% methanol in UPW for 30 minutes.[28] NaCl was extracted in UPW for 2 days. Scaffolds were cut into disks of 3-mm height, punched with a 5-mm diameter biopsy punch, and autoclaved in phosphate buffered saline (PBS) at 121°C for 20 min.

2.4 | Cell culture and seeding

hBMSC isolation and characterization from human bone marrow (Lonza, Walkersville, MD) was performed as previously described.[29] Passage 5 hBMSCs were expanded, trypsinized, and seeded in control medium (DMEM, 10% FBS, and 1% Anti-Anti). Static seeding of hBMSCs involved pipetting a cell suspension (1×10^6 cells/20 μL) onto the pre-wetted scaffolds and incubation for 90 min at 37°C to allow for cell attachment. In the dynamic seeding process, scaffolds were incubated with a cell suspension (1×10^6 cells/4 mL) in 50-mL tubes placed on an orbital shaker at 150 rpm for either 2, 4, or 6 hours in an incubator at 37°C (Figure 2). All scaffolds were incubated in 24-well plates at 37°C and 5% CO_2 for a total of either 24 hours in control medium or 3 weeks in osteogenic medium (control medium with 0.1 μM dexamethasone, 0.05 mM ascorbic acid-2-phosphate, 10 mM β-glycerophosphate).

2.5 | Histology

To analyze the cell distribution, the constructs (n = 5) were fixed in 10% neutral buffered formalin for 24 hours at 4°C and dehydrated with graded ethanol aqueous solutions. The constructs were subsequently soaked in xylene, embedded in paraffin wax, and bisected through the center. Sections (thickness, 5 μm) were prepared from each sample with a microtome (Leica, Germany), deparaffinized, rehydrated in water, treated with 4′,6-diamidino-2-phenylindole for 5 minutes, washed in PBS, mounted in Mowiol, and visualized with a fluorescence microscope (Axiovert 200M; Zeiss

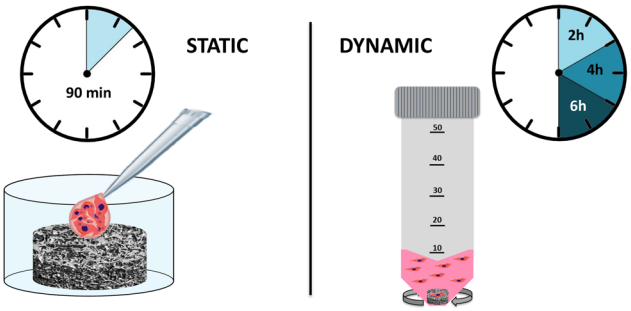

FIGURE 2 Schematic representation of cell seeding. Static seeding of human bone marrow–derived mesenchymal stromal cells (hBMSCs) involved pipetting a cell suspension onto silk fibroin (SF) scaffolds and incubation for 90 minutes at 37°C to allow for cell attachment. In the dynamic seeding process, scaffolds were incubated with a cell suspension in 50-mL tubes placed on an orbital shaker at 150 rpm for either 2, 4, or 6 hours in an incubator at 37°C [Color figure can be viewed at wileyonlinelibrary.com]

Göttingen, Germany). The scaffold sections were divided into three rectangular parts comprising the top, middle, and bottom part of each construct and converted to a binary image using ImageJ.[30] Particles were counted using the particle analyzer tool of ImageJ (pixel size: 10-150). To assess mineral formation in the SF scaffold after 3 weeks of culture, histological sections were deparaffinized, rehydrated in water, and stained with Alizarin red.

2.6 | Microcomputed tomography analysis

μCT measurements were performed on a μCT80 imaging system (Scanco Medical, Brüttisellen, Switzerland) after 3 weeks of culture (n = 4 per group). Scanning was performed at an isotropic nominal resolution of 18 μm, energy level was set to 45 kVp, intensity to 177 μA, 200 microsecond integration time, and two-fold frame averaging. A constrained Gaussian filter was applied to reduce part of the noise. Filter support was set to 1.0 and filter width sigma to 0.8. Segmentation was performed to distinguish mineralized tissue from nonmineralized tissue. A threshold of 22% of the maximal grayscale value was used after visual judgment of the gray images to identify mineralized structures. Components, smaller than 50 voxels, were filtered out through component labeling. Quantitative morphometry was performed to assess relative mineralized ECM volume of the entire construct using direct microstructural bone analysis as previously described for human bone biopsies.[31]

2.7 | DNA content and alkaline phosphatase activity

After culture, scaffolds of all groups (n = 4 per group) were washed in PBS and disintegrated in 0.5 mL of 0.2% (v/v) Triton X-100 and 5 mM $MgCl_2$ solution using steel beads and a Mini Beadbeater™ (Biospec). To determine the DNA content of the initially cells seeded onto the scaffold, 1×10^6 cells were lysed together with a scaffold and processed as the cell seeded constructs. The solids were separated by centrifugation at 3000*g* for 10 minutes. In a 96-well plate, 80 μL of the supernatant was mixed with 20 μL of 0.75M 2-amino-2-methyl-1-propanol buffer and 100 μL 100 mM p-nitrophenylphosphate solution and incubated for 1 minute, before adding 100 μL 0.2M NaOH. Absorbance was measured at 405 nm. After 48 hours of incubation, the DNA content of the supernatant used for the alkaline phosphatase (ALP) assay was determined using the Quant-iT PicoGreen dsDNA Assay Kit according to the manufacturer's instructions. The calculated ALP activity was normalized by the DNA content. DNA amounts per cell were considered constant.

2.8 | Statistical analysis

Quantitative data are represented as mean ± standard deviation. R version 3.3.3 was used for the evaluation of statistically significant differences for ALP assay, DNA assay, and quantitative μCT data. For cell distribution data, the Shapiro–Wilk test confirmed that the data were normally distributed. Homogeneity of variance was confirmed by the Levene test. Analysis of variance was performed followed by post-hoc assessment using the Bonferroni method. For DNA, ALP, and μCT analysis, a Kruskal–Wallis test with Dunn post-hoc testing adjusted by the Benjamini–Hochberg false discovery rate method was performed. Differences between groups were considered statistically significant at a level of $P < .05$. Histological figures show representative images per group of all the samples assessed. μCT images show upper median samples.

3 | RESULTS

3.1 | Shear stress during dynamic seeding

The model predicted the highest shear stress at the periphery of the scaffold (Figure 3A,B; 2.0-2.5 mPa: 8.15%, 2.5-3 mPa: 2.96%, >3 mPa: 3.14%). The majority of the scaffold was exposed to shear stresses of 0-2 mPa (0.0-0.5 mPa: 22.70%, 0.5-1.0 mPa: 18.50%, 1.0-1.5 mPa: 25.05%, 1.5-2.0 mPa: 24.97%). The shear stress was lower in the upper part of the central scaffold region than in the lower part (Figure 3A).

3.2 | Dynamic seeding increases cell density

The effect of static and dynamic seeding on the amount of cells present in SF scaffolds was investigated by analyzing the cell number through the DNA content. Dynamic seeding over a time span of 6 hours resulted in significantly higher cell density than static seeding (static: 23 ± 3 ng, dynamic 6 hours: 58 ± 4 ng; Figure 4). Dynamic seeding for 6 hours gave the cells more time to attach to the scaffold and led to a significantly higher cell density than dynamic seeding for 2 hours (dynamic 2 hours: 28 ± 5 ng; Figure 4). Constructs seeded

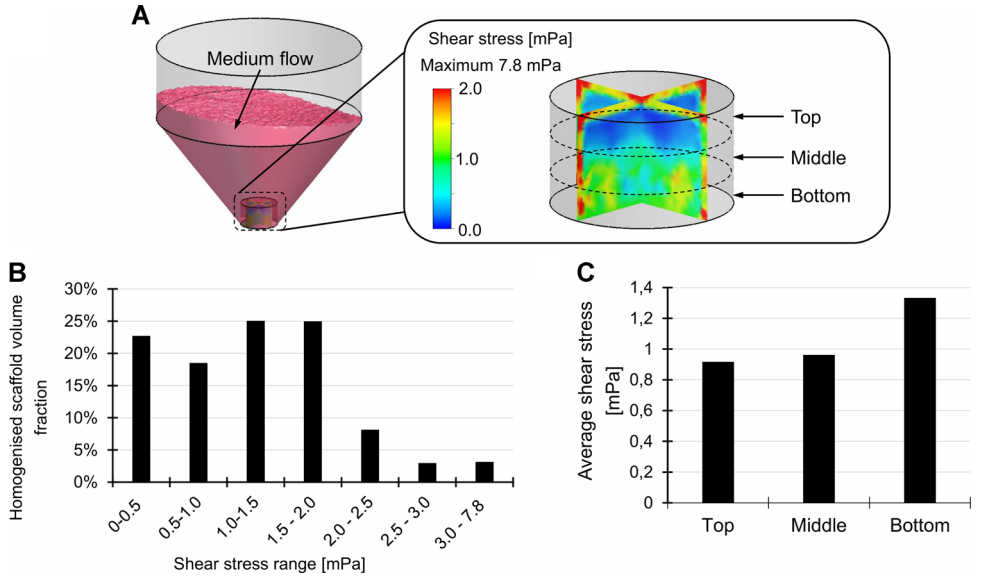

FIGURE 3 Computational results of the orbital shaking system. Dynamic medium flow within the tube and shear stress distribution within the homogenized scaffold (A). Volume fractions of homogenized scaffold which experience different ranges of shear stress (B) [Color figure can be viewed at wileyonlinelibrary.com]

dynamically for 4 hours (44 ± 5 ng) showed no significant differences. Both static seeding and dynamic seeding for 2 hours had significantly less DNA content than the 1×10^6 cells in the control group, which indicates high cell loss during seeding.

3.3 | Dynamic seeding leads to a more homogeneous cell distribution

Cell distribution was analyzed by counting cell nuclei in histological sections. In static samples, most of the cells were accumulated on top of the scaffold (69 ± 5%) while only few cells infiltrated the middle (26 ± 5%) and bottom (6 ± 1%) parts (Figure 5). In comparison to the static group, dynamically seeded constructs showed a more homogeneous distribution regardless of seeding duration (Figure 4B-D). But still, most of the seeded cells accumulated in the top (2 hours: 39 ± 9%, 4 hours: 40 ± 5%, 6 hours: 41 ± 7%) and middle (2 hours: 42 ± 7%, 4 hours: 41 ± 4%, 6 hours: 42 ± 5%) parts. Significantly lower amounts of seeded cells were observed in the bottom part of the constructs (2 hours: 19 ± 4%, 4 hours: 19 ± 3%, 6 hours: 17 ± 4%).

3.4 | Dynamic seeding leads to increased mineralized tissue formation

Mineralization was measured using μCT imaging after 3 weeks. Static seeding produced minor mineralization at the top part of the scaffold. Constructs seeded dynamically showed a more homogeneously distributed mineralization throughout the volume (Figure 6A). The centers of the scaffolds lacked mineral formation, which might be attributed to the diffusion limit of nutrients to and waste from cells in a static culture. Dynamic seeding for 6 and 4 hours resulted in a significantly higher mineral volume than static seeding but not significantly higher than dynamic seeding for 2 hours (static: 0.002 ± 0.001 mm^3, dynamic 2 hours: 0.214 ± 0.091 mm^3, dynamic 4 hours: 0.939 ± 0.171 mm^3, dynamic 6 hours: 1.890 ± 0.831 mm^3; Figure 6B). Cells in statically seeded constructs did not deposit any mineral up to 6 weeks while dynamically seeded constructs increased their mineralized volume over the following 3 weeks (Figure S1). Increased dynamic seeding times showed a trend toward more mineral deposition per initially seeded amount of cells, but that was not statistically significant (Figure S2). However, after 6 weeks of culture, dynamic seeding over 4 and 6 hours resulted in significantly more deposited mineral per cells present in the construct than static seeding and dynamic seeding for 2 hours (Figure 6C). After 3 weeks of culture, histological sections of the constructs were stained for mineral

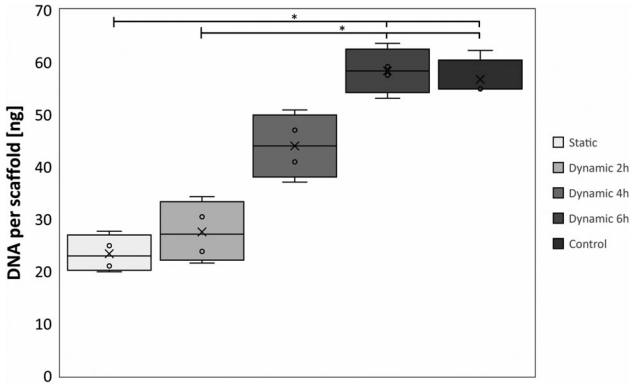

FIGURE 4 DNA assay to determine the number of hBMSCs seeded into SF scaffolds. Cells were seeded either statically or dynamically using an orbital shaker. Dynamic seeding for 6 hours led to a significantly higher cell density than dynamic seeding for 2 hours and static seeding. As a control, the DNA content of 10^6 cells was analyzed. *$P < .05$. hBMSC, human bone marrow–derived mesenchymal stromal cell; SF, silk fibroin

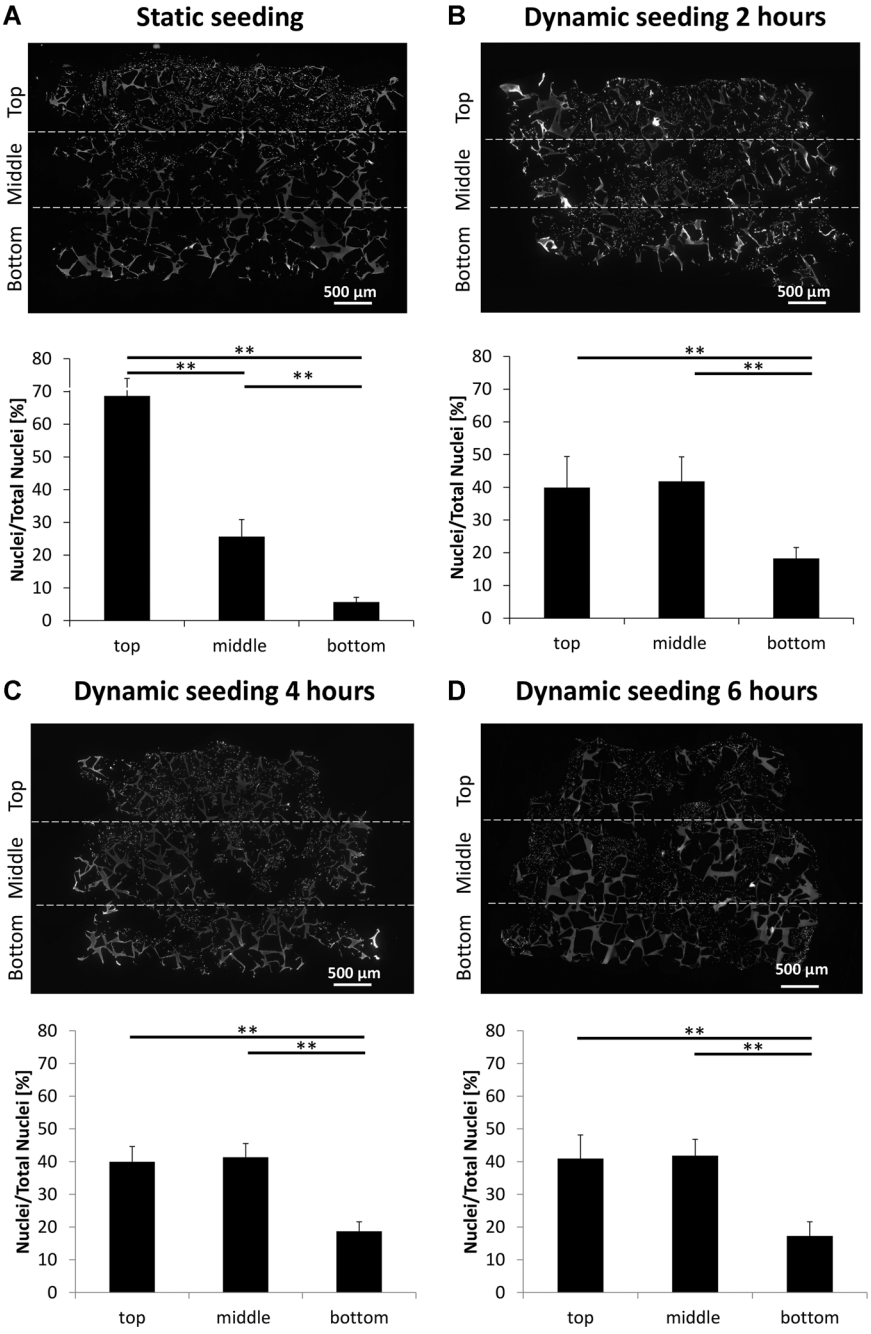

FIGURE 5 Analysis of cell distribution in SF scaffolds seeded statically or dynamically using an orbital shaker. In static samples, most of the cells were accumulated on top of the scaffold while only few cells infiltrated the middle and bottom part (A). Dynamically seeded constructs showed a more homogeneous distribution regardless of seeding duration (B-D). *$P < .05$, **$P < .01$. SF, silk fibroin

deposition. The Alizarin Red staining for mineralization confirmed the observations made with the µCT. Statically seeded constructs showed only minor mineralization while dynamically seeded constructs showed mineral deposition throughout the construct (Figure 7). Statically seeded constructs showed denser tissue formation, especially in the top part of the scaffold (Figure 7A).

3.5 | Dynamic seeding increases ALP activity

Interestingly, after 6 weeks of culture, statically seeded constructs showed a significantly higher cell content per scaffold than constructs seeded dynamically for 2 hours (static: 57 ± 12 ng, dynamic 2 hours: 21 ± 3 ng). Dynamic seeding for 4 and 6 hours was not significantly different (dynamic 4 hours: 28 ± 5 ng, dynamic 6 hours: 38 ± 8 ng; Figure 8A).

Statically cultured constructs had more than double the amount of cells, which points toward an increased cell proliferation. ALP activity was analyzed after 6 weeks of culture and normalized to the cell content and incubation time. Statically seeded constructs had a low amount of ALP, which was less than half of the ALP amount in dynamically seeded constructs (static: 0.78 ± 0.16 µmol·µg^{-1}·min^{-1}, dynamic 2 hours: 2.14 ± 0.19 µmol·µg^{-1}·min^{-1}, dynamic 4 hours: 2.03 ± 0.31 µmol·µg^{-1}·min^{-1}, dynamic 6 hours: 1.95 ± 0.20 µmol·µg^{-1}·min^{-1}; Figure 8B). Statically seeded constructs were significantly different from constructs seeded dynamically for 2 hours.

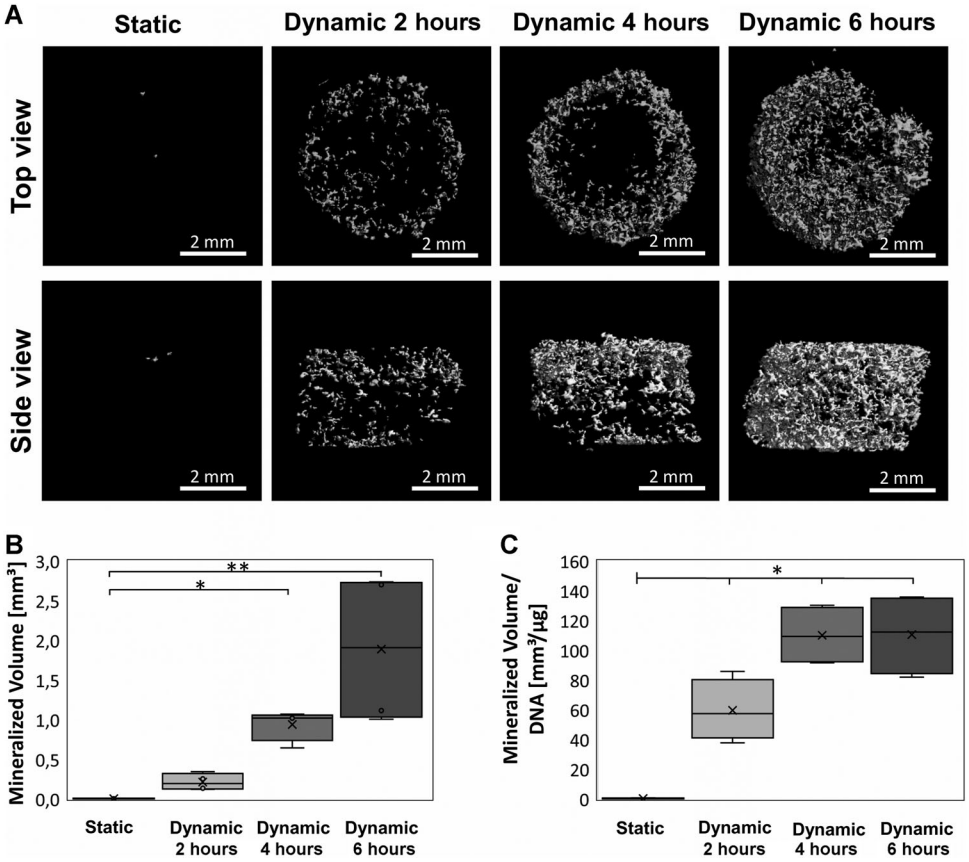

FIGURE 6 µCT of mineralized volume formation of SF scaffolds seeded with hBMSCs and cultured in osteogenic medium. After 3 weeks, static seeding produced minor mineralization at the top part of the scaffold while dynamic seeding showed a more homogeneously distributed mineralization (A). Dynamic seeding for 4 and 6 hours resulted in a significantly higher volume of mineralized extracellular matrix than static seeding (B). After 6 weeks of culture, static seeding resulted in significantly less deposited mineral per amount of cells than dynamic seeding (C). *$P < .05$, **$P < .01$. hBMSC, human bone marrow–derived mesenchymal stromal cell; SF, silk fibroin

4 | DISCUSSION

Guiding cell behavior on scaffolds provides the key to ensuring ultimate functionality in tissue-engineered constructs. It is specifically important to understand how the selection of a seeding method affects cell behavior and ultimate tissue development as well as test cell seeding techniques for their applicability in specific TE fields. In the present study, we demonstrate that a large number of cells can be seeded successfully into porous SF scaffolds using a simple, dynamic seeding approach with an orbital shaker and that dynamic seeding of hBMSCs results in higher osteogenic differentiation than with a static seeding approach.

Cell distribution and density throughout the scaffold after seeding is critical for tissue development. Static seeding was characterized by an inhomogeneous cell distribution as compared to the dynamic seeding approach. In static seeding, cells entered the scaffold because of natural precipitation by gravity. For scaffolds with a pore diameter between 250

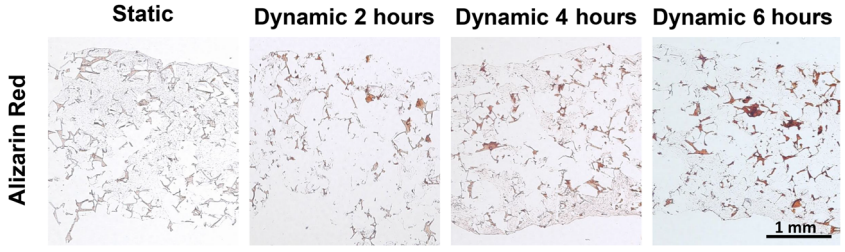

FIGURE 7 Alizarin Red staining for mineralization of SF scaffolds seeded with hBMSCs after 3 weeks of culture in osteogenic medium. Statically seeded constructs showed only minor mineralization while dynamically seeded constructs showed mineral deposition throughout the construct. Mineralization increased with longer seeding times in the dynamic seeding group. hBMSC, human bone marrow–derived mesenchymal stromal cell; SF, silk fibroin [Color figure can be viewed at wileyonlinelibrary.com]

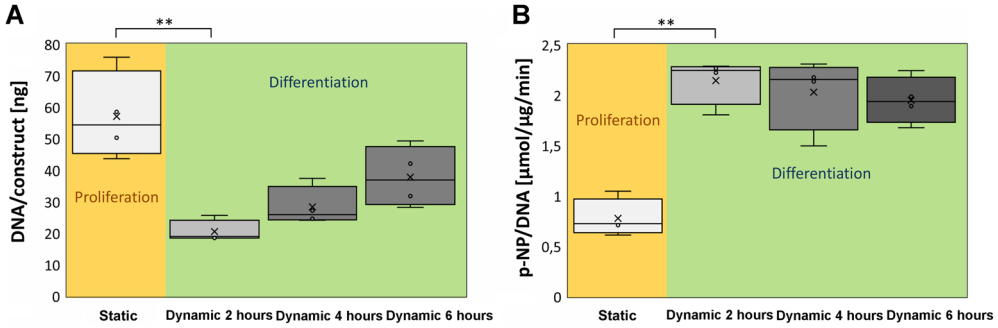

FIGURE 8 DNA and alkaline phosphatase (ALP) assay of SF scaffolds seeded with hBMSCs after 6 weeks of culture in osteogenic medium. Statically cultured constructs had a higher cell content compared to constructs seeded dynamically for 2 hours which suggests an increased cell proliferation (A). Statically seeded constructs showed significantly lower amounts of ALP per cell than constructs seeded dynamically for 2 hours, which indicates that the dynamic group differentiated along the osteogenic lineage (B). $^{**}P < .01$. hBMSC, human bone marrow–derived mesenchymal stromal cell; SF, silk fibroin [Color figure can be viewed at wileyonlinelibrary.com]

and 300 µm as used here, most of the cells pipetted onto the scaffold only entered the upper half of the scaffold. It is likely that the initial cell density and the spatial distribution of cells in the cell-seeded construct impact the growth of engineered tissue in terms of cell proliferation, ECM deposition, and tissue structure, all of which are critical to the construct's functionality. Many reports have highlighted the importance of cell organization, orientation, and differentiation state in dictating tissue-engineering implant functionality.[32–34] A homogenous distribution of cells throughout the scaffold and across the exterior surfaces will lead to the most efficient distribution, growth, and infiltration.

Not only cell-seeding density was enhanced through the use of an orbital shaker, but also the bone-tissue forming capacity. This suggests that prolonged orbital shaking can promote bone tissue formation during subsequent culture and that different seeding methods have the potential to prime cells toward either the proliferative or the differentiation state. As shown by the computational simulation, dynamic seeding could contribute to the bone forming capacity by providing mechanical stimulation through fluid-induced shear stresses in the construct. To quantify the shear stress, we have used a homogenized scaffold model based on Darcy's law, according to our previous study.[19] While this approach saves computation costs, the inhomogeneity of the scaffold permeability and random scaffold geometry may cause a variation of local shear stresses. This factor should be considered in the future applications of the computational model to determine the orbital shaking speed for dynamic cell seeding into scaffolds more precisely, avoid local excessively low or high mechanical stimulation, or even to correlate the local shear stresses with the location of the secreted mineralized ECM. Shear stresses in the scaffold were calculated to be in the range of 0.0 to 3.0 mPa. Mechanical stimulation using fluid-induced shear stress is known to enhance osteogenesis of both osteoblasts and hBMSCs.[35,36] Shear stresses of 1 mPa have been shown to result in an increased osteo-related messenger RNA expression in MC3T3-E1 cells seeded on bone scaffolds.[37] We have previously demonstrated that wall shear stresses in a range of 0.55 to 10 mPa result in tissue-engineered bone formation in 3D SF scaffolds seeded with hBMSCs.[18] However, these bone TE studies focus on mechanical stimulation of constructs during cell culture. The influence of relevant mechanical stimuli during seeding as an isolated factor and what impact it can have on bone-like tissue development in vitro have not been investigated so far.

Another possible explanation for the success of dynamic seeding could be the supply of nutrients. During static seeding, the cells are pipetted onto the scaffold in a highly concentrated cell suspension with little medium and incubated to allow for cell attachment. During this attachment phase, nutrients can be depleted quickly. Limited nutrient supply during early time periods can lead to permanent deleterious effects in the developing tissue.[38–40] During dynamic seeding, cells are permanently provided with cell culture medium.

Even though the inhomogeneous distribution of cells in the static group led to an increased cell density in the top part of the scaffolds, there was only minor mineralized matrix deposition in the upper scaffold region in the static group. This could be attributed, as discussed previously, to a reduced availability of nutrients and/or oxygen during seeding, lack of mechanical stimuli, or subsequent migration of cells toward empty pores.[41]

Mineralized matrix formation was increased toward the exterior of the scaffolds. An open, permeable network architecture with even bigger pores dimensions than used in this study could improve nutrient and oxygen availability during culturing.[42] In static cultures, cells in the center of the scaffold that are too far from the periphery often become necrotic due to hypoxia and lack of nutrients.[43] As a result of these diffusion constraints, only the growth of tissues with cross-sections of less than approximately 400 µm have proven successful in static culture.[44,45] Cell colonization and tissue development at the scaffold periphery due to static seeding, as has been seen also in this study, can act as a barrier and decrease the diffusion of oxygen and nutrients into the interior of the scaffold. This also plays an important role for simulating and adjusting fluid flow during subsequent perfusion cultures.[46]

To further improve the cell seeding process and tissue development, scaffold architecture and physical properties of the scaffolding material should be taken into account.[16,47,48] Inverse opal poly(D, L-lactide-co-glycolide) scaffolds with a uniform pore size and structure increased the seeding efficiency, showed a higher diffusion rate, a uniform distribution

of cells, and a higher degree of differentiation as compared to a non-uniform pore size and structure.[49] Statically seeded SF inverse opal scaffolds seeded with hBMSCs in osteogenic medium showed almost twice as much ECM mineralization as salt-leached SF scaffolds used in the present study.[50]

In summary, we have demonstrated the feasibility of a dynamic seeding method which is simple to use, for bone TE applications. Dynamically seeded constructs were characterized by high cell density, homogeneous cell distribution, increased osteogenic differentiation, and higher mineral deposition. This simple seeding technique has the potential to be applied in other TE fields and is recommended to be used for seeding similar porous scaffolds with hBMSCs.

5 | CONCLUSION

In this study, we have demonstrated that the use of a simple, dynamic seeding method using an orbital shaker leads to significantly higher numbers of hBMSCs and a homogenous cell distribution inside a SF scaffold than static seeding. The dynamic seeding method led to a homogeneous tissue development, increased osteogenic differentiation of hBMSCs, and increased mineral deposition in the constructs. The positive influence of dynamic seeding may be attributed to the increased cell density and homogeneous cell distribution but also increased nutrient supply during seeding and mechanical forces. The influence of relevant mechanical stimuli such as shear stress during seeding should be investigated in the future, especially regarding the importance of mechanical cues for bone TE application. Our results highlight the importance of adequate choice of seeding method and its impact on the developing tissue-engineered constructs. The application of this simple seeding technique is not only recommended for bone TE but can also be used for seeding similar porous scaffolds with hBMSCs in other TE fields.

ACKNOWLEDGMENT

This project was supported by the European Union's Seventh Framework Programme (FP/2007-2013)/grant agreement No. 336043.

AUTHOR CONTRIBUTION

JM and SH participated in the conception and design of this study. JM preformed the cell cultures experiments and acquired data. FZ performed the computational simulations. JM, FZ, KI, and SH participated in analysis and interpretation of the data. JM and FZ drafted the manuscript. Revisions and final approval of manuscript were made by JM, FZ, KI, and SH.

ORCID

Johanna Melke http://orcid.org/0000-0002-4858-2092
Feihu Zhao http://orcid.org/0000-0003-0515-6808
Sandra Hofmann http://orcid.org/0000-0002-2568-8388

REFERENCES

1. Henkel J, Woodruff MA, Epari DR, et al. Bone regeneration based on tissue engineering conceptions—A 21st century perspective. *Bone Res*. 2013;1:216-248. https://doi.org/10.4248/BR201303002
2. Black CRM, Goriainov V, Gibbs D, Kanczler J, Tare RS, Oreffo ROC. Bone tissue engineering. *Curr Mol Biol Reports*. 2015;1(3):132-140. https://doi.org/10.1007/s40610-015-0022-2
3. Amini AR, Laurencin CT, Nukavarapu SP. Bone tissue engineering: Recent advances and challenges. *Crit Rev Biomed Eng*. 2012;40(5):363-408. http://www.ncbi.nlm.nih.gov/pmc/articles/PMC3766369/
4. Kruyt M, De Bruijn J, Rouwkema J, et al. Analysis of the dynamics of bone formation, effect of cell seeding density, and potential of allogeneic cells in cell-based bone tissue engineering in goats. *Tissue Eng Part A*. 2008;14(6):1081-1088.
5. Hasegawa T, Miwa M, Sakai Y, et al. Efficient cell-seeding into scaffolds improves bone formation. *J Dent Res*. 2010;89(8):854-859.
6. Yassin MA, Leknes KN, Pedersen TO, et al. Cell seeding density is a critical determinant for copolymer scaffolds-induced bone regeneration. *J Biomed Mater Res A*. 2015;103(11):3649-3658.
7. Li Y, Ma T, Kniss DA, Lasky LC, Yang ST. Effects of filtration seeding on cell density, spatial distribution, and proliferation in nonwoven fibrous matrices. *Biotechnol Prog*. 2001;17(5):935-944.
8. Wendt D, Marsano A, Jakob M, Heberer M, Martin I. Oscillating perfusion of cell suspensions through three-dimensional scaffolds enhances cell seeding efficiency and uniformity. *Biotechnol Bioeng*. 2003;84(2):205-214.
9. Thevenot P, Nair A, Dey J, Yang J, Tang L. Method to analyze three-dimensional cell distribution and infiltration in degradable scaffolds. *Tissue Eng Part C Methods*. 2008;14(4):319-331. http://www.pubmedcentral.nih.gov/articlerender.fcgi?artid=2913783&tool=pmcentrez&rendertype=abstract
10. Meinel L, Hofmann S, Betz O, et al. Osteogenesis by human mesenchymal stem cells cultured on silk biomaterials: comparison of adenovirus mediated gene transfer and protein delivery of BMP-2. *Biomaterials*. 2006;27(28):4993-5002. http://www.ncbi.nlm.nih.gov/pubmed/16765437
11. Solchaga LA, Tognana E, Penick K, et al. A rapid seeding technique for the assembly of large cell/scaffold composite constructs. *Tissue Eng*. 2006;12(7):1851-1863.
12. Kitagawa T, Yamaoka T, Iwase R, Murakami A. Three-dimensional cell seeding and growth in radial-flow perfusion bioreactor for in vitro tissue reconstruction. *Biotechnol Bioeng*. 2006;93(5):947-954. https://doi.org/10.1002/bit.20797
13. Wendt D, Stroebel S, Jakob M, John GT, Martin I. Uniform tissues engineered by seeding and culturing cells in 3D scaffolds under perfusion at defined oxygen tensions. *Biorheology*. 2006;43(3–4):481-488.
14. Xie J, Jung Y, Kim SH, Kim YH, Matsuda T. New technique of seeding chondrocytes into microporous poly(L-lactide-co-epsilon-caprolactone) sponge by cyclic compression force-induced suction. *Tissue Eng*. 2006;12(7):1811-1820.
15. Unsworth JM, Rose FRAJ, Wright E, Scotchford CA, Shakesheff KM. Seeding cells into needled felt scaffolds for tissue engineering applications. *J Biomed Mater Res A*. 2003;66(2):425-431.
16. Alvarez-Barreto JF, Linehan SM, Shambaugh RL, Sikavitsas VI. Flow perfusion improves seeding of tissue engineering scaffolds with different architectures. *Ann Biomed Eng*. 2007;35(3):429-442.
17. Shimizu K, Ito A, Honda H. Mag-seeding of rat bone marrow stromal cells into porous hydroxyapatite scaffolds for bone tissue engineering. *J Biosci Bioeng*. 2007;104(3):171-177.
18. Melke J, Zhao F, van Rietbergen B, Ito K, Hofmann S. Localisation of mineralised tissue in a complex spinner flask environment correlates with predicted wall shear stress level localisation. *Eur Cell Mater*. 2018;36:57-68.
19. Zhao F, Melke J, Ito K, van Rietbergen B, Hofmann S. A multiscale computational fluid dynamics approach to simulate the micro-fluidic

environment within a tissue engineering scaffold with highly irregular pore geometry. *Biomech Model Mechanobiol*. 2019;18(6):1965-1977.
20. Guyot Y, Papantoniou I, Luyten FP, Geris L. Coupling curvature-dependent and shear stress-stimulated neotissue growth in dynamic bioreactor cultures: a 3D computational model of a complete scaffold. *Biomech Model Mechanobiol*. 2016;15(1):169-180.
21. Guyot Y, Luyten FP, Schrooten J, Papantoniou I, Geris L. A three-dimensional computational fluid dynamics model of shear stress distribution during neotissue growth in a perfusion bioreactor. *Biotechnol Bioeng*. 2015;112(12):2591-2600.
22. Maisonneuve BGC, Roux DCD, Thorn P, Cooper-White JJ. Effects of cell density and biomacromolecule addition on the flow behavior of concentrated mesenchymal cell suspensions. *Biomacromolecules*. 2013; 14:4388-4397.
23. Cherng WJ, Dong ZS, Chou CC, Yeh YHP. CH. Three dimensional geological modeling as a cost effective tool for horizontal drilling. *Micromachines*. 2017;8(132):1-9.
24. Salek MM, Sattari P, Martinuzzi RJ. Analysis of fluid flow and wall shear stress patterns inside partially filled agitated culture well plates. *Ann Biomed Eng*. 2012;40(3):707-728.
25. Thomas JMD, Chakraborty A, Sharp MK, Berson RE. Spatial and temporal resolution of shear in an orbiting petri dish. *Biotechnol Prog*. 2011;27(2):460-465.
26. Meinel L, Fajardo R, Hofmann S, et al. Silk implants for the healing of critical size bone defects. *Bone*. 2005;37(5):688-698. http://www.ncbi.nlm.nih.gov/pubmed/16140599
27. Nazarov R, Jin HJ, Kaplan DL. Porous 3-D scaffolds from regenerated silk fibroin. *Biomacromolecules*. 2004;5(3):718-726. https://doi.org/10.1021/bm034327e
28. Tsukada M, Gotoh Y, Nagura M, Minoura N, Kasai N, Freddi G. Structural changes of silk fibroin membranes induced by immersion in methanol aqueous solutions. *J Polym Sci Part B Polym Phys*. 1994; 32(5):961-968. https://www.scopus.com/inward/record.uri?eid=2-s2.0-0028413371&doi=10.1002%2Fpolb.1994.090320519&partnerID=40&md5=d991b46bb4907c49a9087599eb7ceeba
29. Hofmann S, Hagenmüller H, Koch AM, et al. Control of in vitro tissue-engineered bone-like structures using human mesenchymal stem cells and porous silk scaffolds. *Biomaterials*. 2007;28(6):1152-1162. http://www.ncbi.nlm.nih.gov/pubmed/17092555
30. Schneider CA, Rasband WS, Eliceiri KW. NIH Image to ImageJ: 25 years of image analysis. *Nat Methods*. 2012;9:671-675. https://doi.org/10.1038/nmeth.2089
31. Hildebrand T, Laib A, Müller R, Dequeker J, Rüegsegger P. Direct three-dimensional morphometric analysis of human cancellous bone: microstructural data from spine, femur, iliac crest, and calcaneus. *J Bone Miner Res*. 1999;14(7):1167-1174.
32. Martin I, Wendt D, Heberer M. The role of bioreactors in tissue engineering. *Trends Biotechnol*. 2004;22(2):80-86. http://www.ncbi.nlm.nih.gov/pubmed/14757042
33. Lutolf MP, Hubbell JA. Synthetic biomaterials as instructive extracellular microenvironments for morphogenesis in tissue engineering. *Nat Biotechnol*. 2005;23(1):47-55.
34. Takezawa T. A strategy for the development of tissue engineering scaffolds that regulate cell behavior. *Biomaterials*. 2003;24(13):2267-2275.
35. Kapur S, Baylink DJ, Lau KH. Fluid flow shear stress stimulates human osteoblast proliferation and differentiation through multiple interacting and competing signal transduction pathways. *Bone*. 2003; 32(3):241-251. http://www.sciencedirect.com/science/article/pii/S8756328202009791
36. Yourek G, McCormick SM, Mao JJ, Reilly GC. Shear stress induces osteogenic differentiation of human mesenchymal stem cells. *Regen Med*. 2010;5(5):713-724.
37. Porter B, Zauel R, Stockman H, Guldberg R, Fyhrie D. 3-D computational modeling of media flow through scaffolds in a perfusion bioreactor. *J Biomech*. 2005;38(3):543-549. http://www.sciencedirect.com/science/article/pii/S0021929004001964
38. Stephan S, Johnson WE, Roberts S. The influence of nutrient supply and cell density on the growth and survival of intervertebral disc cells in 3D culture. *Eur Cell Mater*. 2011;22:97-108.
39. Mauck RL, Wang CCB, Oswald ES, Ateshian GA, Hung CT. The role of cell seeding density and nutrient supply for articular cartilage tissue engineering with deformational loading. *Osteoarthr Cartil*. 2003;11(12): 879-890.
40. Oskowitz A, McFerrin H, Gutschow M, Carter ML, Pochampally R. Serum-deprived human multipotent mesenchymal stromal cells (MSCs) are highly angiogenic. *Stem Cell Res*. 2011;6(3):215-225. http://www.sciencedirect.com/science/article/pii/S1873506111000055
41. Li X, Dai Y, Shen T, Gao C. Induced migration of endothelial cells into 3D scaffolds by chemoattractants secreted by pro-inflammatory macrophages in situ. *Regen Biomater*. 2017;4(3):139-148.
42. Di Luca A, Ostrowska B, Lorenzo-Moldero I, et al. Gradients in pore size enhance the osteogenic differentiation of human mesenchymal stromal cells in three-dimensional scaffolds. *Sci Rep*. 2016;6:22898. https://doi.org/10.1038/srep22898
43. Volkmer E, Drosse I, Otto S, et al. Hypoxia in static and dynamic 3D culture systems for tissue engineering of bone. *Tissue Eng Part A*. 2008;14(8):1331-1340.
44. Ishaug-Riley SL, Crane GM, Gurlek A, et al. Ectopic bone formation by marrow stromal osteoblast transplantation using poly(DL-lactic-co-glycolic acid) foams implanted into the rat mesentery. *J Biomed Mater Res*. 1997;36(1):1-8.
45. Rouwkema J, Koopman BFJM, Blitterswijk CAV, Dhert WJA, Malda J. Supply of nutrients to cells in engineered tissues. *Biotechnol Genet Eng Rev*. 2010;26:163-178.
46. Martin I, Padera RF, Vunjak-Novakovic G, Freed LE. In vitro differentiation of chick embryo bone marrow stromal cells into cartilaginous and bone-like tissues. *J Orthop Res*. 1998;16(2):181-189.
47. Melchels FPW, Barradas AMC, van Blitterswijk CA, de Boer J, Feijen J, Grijpma DW. Effects of the architecture of tissue engineering scaffolds on cell seeding and culturing. *Acta Biomater*. 2010;6(11):4208-4217.
48. Olivares AL, Lacroix D. Simulation of cell seeding within a three-dimensional porous scaffold: A fluid-particle analysis. *Tissue Eng Part C Methods*. 2012;18(8):624-631.
49. Choi SW, Zhang Y, Xia Y. Three-dimensional scaffolds for tissue engineering: The importance of uniformity in pore size and structure. *Langmuir*. 2010;26(24):19001-19006.
50. Sommer MR, Vetsch JR, Leemann J, Müller R, Studart AR, Hofmann S. Silk fibroin scaffolds with inverse opal structure for bone tissue engineering. *J Biomed Mater Res B Appl Biomater*. 2016;105:2074-2084.

SUPPORTING INFORMATION

Additional supporting information may be found online in the Supporting Information section.

How to cite this article: Melke J, Zhao F, Ito K, Hofmann S. Orbital seeding of mesenchymal stromal cells increases osteogenic differentiation and bone-like tissue formation. *J Orthop Res*. 2020;38:1228–1237. https://doi.org/10.1002/jor.24583